Proceedings of the European Conference "Physics of Magnetism" (PM'08), Poznań 2008

Pressure Effect on Yb-Based Strongly Correlated Electron Systems

T. Mito*, M. Otani, M. Nakamura, T. Koyama*, S. Wada
Graduate School of Sciences, Kobe University, Nada, Kobe 657-8501, Japan
H. Kotegawa†, T.C. Kobayashi
Graduate School of Sciences, Okayama University, Okayama 700-8530, Japan
B. Idzikowski
Institute of Molecular Physics, Polish Academy of Sciences
60-179 Poznań, Poland
M. Reiffers
Institute of Experimental Physics, Slovak Academy of Sciences
043-53 Kosice, Slovakia
and J.L. Sarrao
Los Alamos National Laboratory, Mail Stop K764
Los Alamos, New Mexico 87545, USA

We studied pressure effects on $YbCu_5$ and $YbInCu_4$, good examples of the Yb-based compounds to investigate the nonmagnetic–magnetic transition in Yb-based strongly correlated electron systems. With increasing pressure, the low-temperature Fermi liquid state of $YbCu_5$ is gradually suppressed, suggesting the second-order like nonmagnetic–magnetic transition around the pressure of 5–6 GPa. On the other hand, in $YbInCu_4$ which has a pressure-induced magnetic ordered ground state above $P_C = 2.45$ GPa, both high-temperature paramagnetic and low-temperature intermediate valence phases are insensitive to pressure. Our results confirm the first-order nature of the transition between the intermediate valence and magnetic ordered phases with pressure.

PACS numbers: 71.27.+a, 75.30.Kz, 75.30.Mb, 76.60.–k

1. Introduction

The study of nonmagnetic–magnetic transitions in f electron systems has been a topic of interest and controversy because of many fascinating physical properties around the boundary, for example unconventional superconductivity. There are indeed a large number of accumulated studies on the Ce-based compounds, especially the investigations crossing a quantum critical point by using pressure or chemical substitution techniques. On the other hand, Yb-based compounds, which are also interesting due to the hole–electron analogy between the $4f^{13}$-Yb^{3+} and the $4f^{1}$-Ce^{3+} electronic configurations, have been rather less investigated.

In this context, a series of $YbXCu_4$ (X = Ag, Au, Cd, Cu, In, Mg, Pd, Tl, Zn), with the $AuBe_5$-type cubic structure ($C15b$), presents the opportunity to study this topic systematically. They exhibit a broad range of ground state, such as mixed valence, heavy fermion, and magnetically ordered states, by changing X atoms. To understand the ground-state properties especially in the nonmagnetic region, the lattice parameter a seems one of the key parameters. In Fig. 1a we plot the values of a at room temperature for only nonmagnetic $YbXCu_4$ compounds, so that a tends to increase in the order X = Cu, Zn, Ag, Cd, In, Tl, and Mg. In the figure, regarding the X = In which shows a phase transition at $T_V = 42$ K, we plot the data for the low-temperature phase, because the high-temperature phase has a magnetically ordered ground state when it is stabilized down to the lowest temperature by pressure [1, 2]. In Fig. 1b the values of the electronic specific heat coefficient γ and the Kondo temperature T_0 are shown in the same order of X with Fig. 1a, which reveals some relation between γ, T_0 and a: γ increases and T_0 decreases as a function of a. This result seems to be plausible, because heavy fermion compounds such as X = Cu prefer relatively localized $4f$ electronic state, namely close

* Present address: Graduate School of Material Science, University of Hyogo, Hyogo 678-1297, Japan.
† Present address: Graduate School of Sciences, Kobe University, Nada, Kobe 657-8501, Japan.

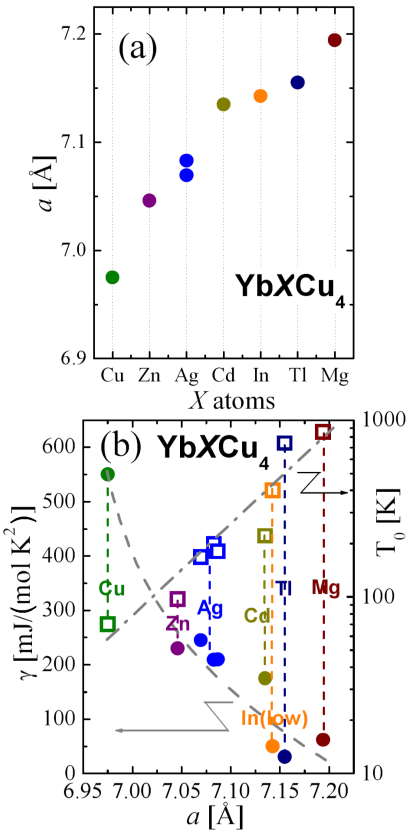

Fig. 1. (a) Lattice constants of $YbXCu_4$ (X = Cu [3], Zn [8], Ag [9, 10], Cd [8], In [11], Tl [8], and Mg [8]). The data are values at room temperature except for X = In for which we plotted the data below T_V. (b) The plots of γ (circles) and T_0 (open squares) versus a for $YbXCu_4$ [3, 8–11].

to the Yb^{3+} state, whereas X = Tl and Mg exhibit mixed valence states involving larger-size Yb^{2+} state. In this paper, we focus on the two compounds which are good candidates to investigate the nonmagnetic–magnetic transition in the Yb-based compounds by using the pressure technique. $YbCu_5$ shows the largest γ of 550 mJ/(mol K^2) among the $YbXCu_4$ compounds in Fig. 1 [3], and it does not show any evidence for magnetic ordering down to $\approx$ 60 mK at ambient pressure [4]. It is therefore expected that this compound is located close to the nonmagnetic–magnetic phase boundary. $YbInCu_4$ is one of the most intensively investigated compounds among $YbXCu_4$, because this undergoes a drastic phase transition at T_V: an isostructural valence transition from a well-localized Yb^{3+} state for $T > T_V$ to an intermediate valence state for $T < T_V$ [5, 6]. The important feature of $YbInCu_4$ for the present study is that this compound shows field-induced magnetic ordering above critical pressure of $P_C \approx 2.45$ GPa [7]. This relatively low P_C, which is achieved with a conventional piston-cylinder type pressure cell, allows one to perform precise studies of the physical properties in the vicinity of the nonmagnetic–magnetic boundary.

2. Experimental details

Early reports on $YbCu_5$ indicated that it had the hexagonal $CaCu_5$-type structure [12, 13], however Tsujii et al. succeeded in stabilizing the cubic $AuBe_5$ structure, regarded as the mother compound of the $YbXCu_4$ system, under pressure [3]. Instead, our present polycrystalline sample was prepared by using single roller melt spinning technique on a copper wheel. This technique allows skipping over the hexagonal-phase-forming region, and $YbCu_5$ with the cubic structure is directly obtained from the liquid state. The details are described in Ref. [14]. The sample has the shape of ribbon with typical dimensions of $\approx$ 50 μm thick, 5–10 mm length, and $\approx$ 3 mm width. X-ray diffraction (XRD) showed that the sample was single phase with the proper cubic $AuBe_5$ structure. The main properties of the sample (resistivity, susceptibility and specific heat) are reported in Ref. [15]. For $YbCu_4$, single crystals were grown using the flux method as described in Ref. [16].

The electrical resistivity was measured by a conventional four probe method. Hydrostatic pressure for the resistivity measurements was applied using an indenter-type pressure cell, filled with Daphne oil (7373) as a pressure-transmitting medium. Pressure at low temperatures was calibrated by the resistivity measurement of a superconducting Pb manometer. The resistivity was measured down to $\approx$ 60 mK using a dilution refrigerator. For the nuclear magnetic resonance (NMR) and nuclear quadrupole resonance (NQR) measurements, a powder sample, in which grain size is a few hundreds μm or less, were used. The NMR/NQR measurements were performed using a phase-coherent spin-echo spectrometer, and the Knight shift was obtained by analyzing the NMR spectrum as a function of field around 3 T. The spin lattice relaxation time T_1 was measured by the single rf-pulse saturation method. Pressure for the NMR/NQR measurements was produced by using a piston-cylinder pressure-cell made of nonmagnetic NiCrAl/CuBe alloy with Daphne oil (7373) as a pressure-transmitting medium. Pressure was monitored by using a superconducting Sn manometer.

3. Results and discussion

3.1. $YbCu_5$

Figure 2 shows the representative temperature dependences of the electrical resistivity $\rho(T)$ measured at different pressures. The temperature dependence at ambient pressure is in good agreement with the previous report on the sample synthesized under high pressure [3], except that the present absolute value is about 2.5 times larger. The larger value of ρ might be due to: (i) there are some disorders introduced on the surface when the sample was quenched during melt spinning; (ii) the thin ribbon of sample does not have uniform thickness, leading to the overestimation of the sample thickness and the resistivity. $\rho(T)$ at ambient pressure has a minimum around 150 K and increases down to $T^{\rho}_{max} \approx 35$ K, which is explained within the framework of the single-site Kondo

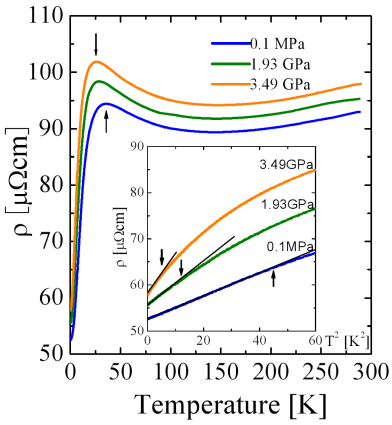

Fig. 2. Representative temperature dependences of $\rho(T)$ at $P = 0.1$, 1.93 and 3.49 GPa. The arrows indicate $T^{\rho}_{\rm max}(P)$ where ρ is a maximum. Inset: plot of ρ vs. T^2 at these pressures. The arrows indicate the temperature $T_{\rm FL}$ below which $\rho(T)$ follows the $\rho(T) \propto T^2$ law.

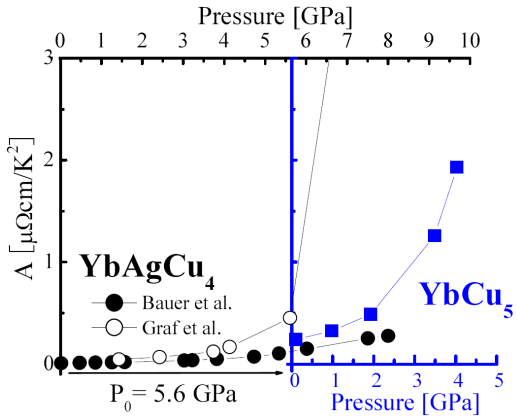

Fig. 3. Pressure dependence of A for $YbCu_5$ (squares) together with the data of $YbAgCu_4$ (circles) [17, 18]. In the figure, the pressure axis (lower scale) for $YbCu_5$ is shifted by chemical pressure $P_0 = 5.6$ GPa with respect to the axis (upper scale) for $YbAgCu_4$. See text for details.

scattering between $4f$ and conduction electrons. $\rho(T)$ exhibits a maximum at $T^{\rho}_{\rm max}$, followed by a significant decrease below $T^{\rho}_{\rm max}$. Because the temperature dependence of $\rho(T)$ changes into the T^2 behavior with further decreasing temperature, as expected in the Fermi liquid regime, the reduction below $T^{\rho}_{\rm max}$ is ascribed to the formation of the Kondo coherent state. The inset of Fig. 2 demonstrates the $\rho(T)$ vs. T^2 plot. The resistivity follows $\rho(T) = \rho_0 + AT^2$ below $T_{\rm FL}$ where $T^2_{\rm FL} \approx 40$ K^2 at ambient pressure. Here ρ_0 is the residual resistivity and A is the coefficient of the quadratic term.

The pressure dependence of A is shown in Fig. 3, in which we compare the result with the data on isostructural relative $YbAgCu_4$ [17, 18]. $YbAgCu_4$ has a slightly smaller lattice constant a as shown in Fig. 1, and it is a moderately heavy fermion compound ($\gamma = 240$ mJ/(mol K^2)) [9]. $\rho(T)$ of $YbAgCu_4$ is qualitatively analogous with that of $YbCu_5$; it also shows $T^{\rho}_{\rm max}$ and T^2 behavior at low temperatures. Since the pressure effect on a and $\rho(T)$ of $YbAgCu_4$ has been intensively studied so far [17, 18], it is useful to compare $YbCu_5$ with $YbAgCu_4$. In Fig. 3 the pressure axis for $YbCu_5$ is shifted by $P_0 = 5.6$ GPa with respect to that for $YbAgCu_4$. Here, the chemical pressure P_0 was evaluated by referring a previous high pressure study on $YbAgCu_4$ [17]; $a = 6.975$ Å of $YbCu_5$ at ambient pressure [3] corresponds to the value of $YbAgCu_4$ at P_0. There are somewhat differences between the $YbAgCu_4$ data from Refs. [17] and [18]. Nevertheless, the pressure dependence of A for $YbCu_5$ rather smoothly connect with those for $YbAgCu_4$, especially the data from Ref. [17], suggesting that $YbCu_5$ has an advantage of $P_0 = 5$–6 GPa in terms of approaching the nonmagnetic--magnetic border by pressure. These results appear consistent with the report that the substitution effect of Ag by Cu in $YbAgCu_4$, which shrinks the unit--cell volume, is mainly explained by chemical pressure effect [10].

Next, we study the pressure effect on the susceptibility χ. Here, our χ data of $YbCu_5$ exhibit sample dependence especially at low temperatures. This is mainly because $\chi(T)$ actually includes contributions from small impurity phases. Therefore, we have measured the Knight shift K, since it is known that K is little influenced by the impurities. Here, K generally linearly depends on χ; $K = (A_{\rm hf}/N_{\rm A}\mu_{\rm B})\chi$, where $A_{\rm hf}$ is the hyperfine coupling constant, and $N_{\rm A}$ is the Avogadro number. Besides, the K measurement has the advantage that the data even above 2 GPa can be obtained by using a conventional pressure cell. K was measured at the ^{63}Cu-4c site, in which the value of K was rather simply determined because the resonance was free from the nuclear quadrupole interactions due to the absence of the local electric-field gradients. We suppose that K reflects the intrinsic temperature dependence of χ by assuming small temperature and pressure dependences of $A_{\rm hf}$.

The K versus χ plot is shown in Fig. 4a, where temperature is an implicit parameter. By using the obtained linear relation above 40 K, we evaluated the temperature dependence of the susceptibility, $\chi^{\rm NMR}(T)$, as shown in Fig. 4b. $\chi^{\rm NMR}(T)$ for $YbCu_5$ is analogous with the temperature dependence of χ for $YbAgCu_4$. At high temperatures, $\chi^{\rm NMR}(T)$ follows the Curie–Weiss law with the effective moment $\mu_{\rm eff} = 4.3$ $\mu_{\rm B}$ and the Weiss temperature $\Theta = -23$ K, indicating a well localized $4f$ electronic state. With decreasing temperature, $\chi^{\rm NMR}(T)$ exhibits a peak around $T^{\chi}_{\rm max} = 20$ K, followed by temperature--invariant dependence, characteristic of the Fermi liquid behavior. $T^{\chi}_{\rm max}$ is hence regarded as the crossover temperature from localized to itinerant coherent Kondo states, consistent with the rapid decrease in ρ below $T^{\rho}_{\rm max}$ (see Fig. 2a). Compared to $\chi(T)$ of $YbAgCu_4$, $\chi^{\rm NMR}(T)$ of $YbCu_5$ follows the Curie–Weiss law down to

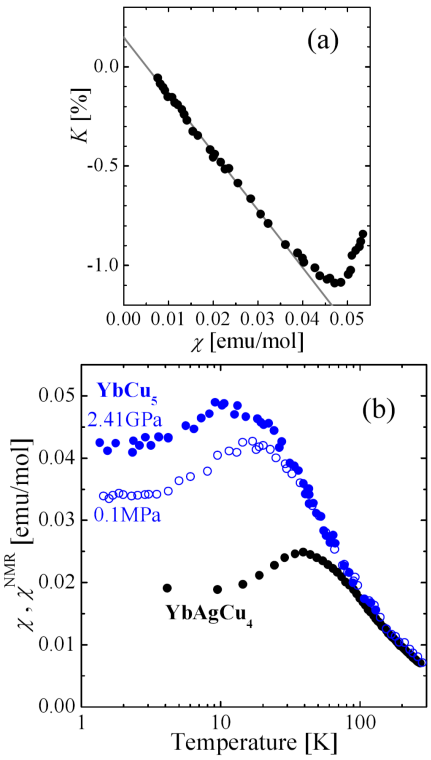

Fig. 4. (a) K versus χ plot at ambient pressure with temperature as an implicit parameter. The solid line is a linear fit to the data above 40 K. (b) Temperature dependence of $\chi^{\rm NMR}$ at ambient pressure and 2.41 GPa along with the susceptibility data for $YbAgCu_4$. Here, $\chi^{\rm NMR}$ was evaluated from the Knight shift data. See text for details.

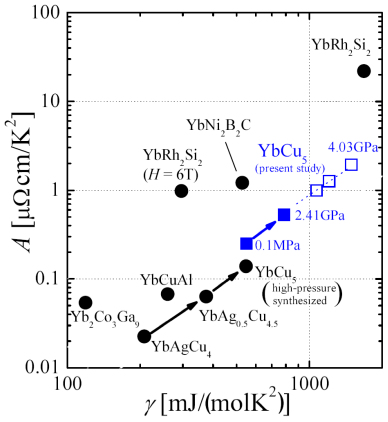

Fig. 5. A vs γ plot obtained from the present experiment (squares), together with the values for other Yb-based compounds (circles) [22]. The arrows indicate the pressure effect for $YbCu_5$ and the substitution effect of Ag by Cu in $YbAg_{1-x}Cu_{4+x}$ [10].

much lower temperature $\approx$ 40 K, implying that $YbCu_5$ is located closer to the magnetic–nonmagnetic border. This trend becomes more remarkable at the pressure of 2.41 GPa, however the characteristic behavior of the Fermi liquid state is still observed at this pressure. Let us note that similar behavior of $\chi(T)$ is also observed when applying field of a few kOe to $YbRh_2Si_2$ which exhibits antiferromagnetic ordering at $T_{\rm N} = 70$ mK. In that case, $T^{\chi}_{\rm max}$ is lower than 1 K [19, 20]. In order to examine how $YbCu_5$ approaches the quantum criticality with pressure, it is useful to show the pressure dependences of γ and A on the Kadowaki–Woods plot [21]. Here, because there is generally a linear relation between γ and $\chi(0)$, $\chi(T)$ at zero temperature, via the Wilson ratio, we can obtain the plausible value of γ under pressure by assuming the constancy of the Wilson ratio with pressure. In Fig. 5, we plot the obtained γ and $\chi(0)$ for $YbCu_5$ with the data of other Yb-based compounds. As pressure is increased up to 2.41 GPa, γ and A are increased with keeping the relation of $A \propto \gamma^2$. However, the pressure of 2.41 GPa, the maximum pressure for the present NMR measurement, is not enough to be close to the quantum criticality, as mentioned above. Then we tentatively plot the A values up to 4.03 GPa, the maximum pressure for the resistivity measurement, by extrapolating the relation of $A \propto \gamma^2$. Interestingly the data approach the right end of the Kadowaki–Woods plot. $T^{\chi}_{\rm max}$ is extrapolated to zero around 5 GPa, a value which is supposed to be the nonmagnetic–magnetic border.

3.2. YbInCu4

The valence transition of $YbInCu_4$ strongly depends on hydrostatic pressure [7, 23–26]. By applying pressure above $P_{\rm C} \approx 2.45$ GPa, the low-temperature intermediate valence (IV) phase is suppressed below 2.5 K and a new magnetically ordered phase appears below $T_{\rm M} \approx 2.4$ K [7, 2]. The features near the pressure-induced nonmagnetic–magnetic transition in this compound have been investigated mainly by the NQR measurements at a microscopic level [1, 27], in which the first-order nature of the valence transition even very close to $P_{\rm C}$ was indicated. However, in those experiments, the onset of the magnetic order was indirectly indicated by the sudden disappearance of the NQR signal below $T_{\rm M}$: the emergence of internal field associated with magnetic ordering gives rise to broadening or shift of the resonance lines.

In the present experiment at 2.5 GPa, we have found significantly broadened NQR signal from the magnetically ordered (MO) phase below $T_{\rm M}$. Figure 6 shows the temperature variations of the Cu-NQR lines as a function of frequency. In the paramagnetic (PM) state above $T_{\rm M}$, for example at 4.2 K as shown in the figure, two resonance lines of ^{65}Cu and ^{63}Cu are observed around 14.3 and 15.5 MHz, respectively. With decreasing temperature below $T_{\rm M}$, the resonance lines from the PM phase become weak. Instead, the observed line shape below $T_{\rm M}$ is a superposition of a set of signals with distinguishable peaks at 14 and 15 MHz and a broad line (see the line at 1.4 K in the figure). The former is assigned to signals from the IV phase [1], and the latter is ascribed to the

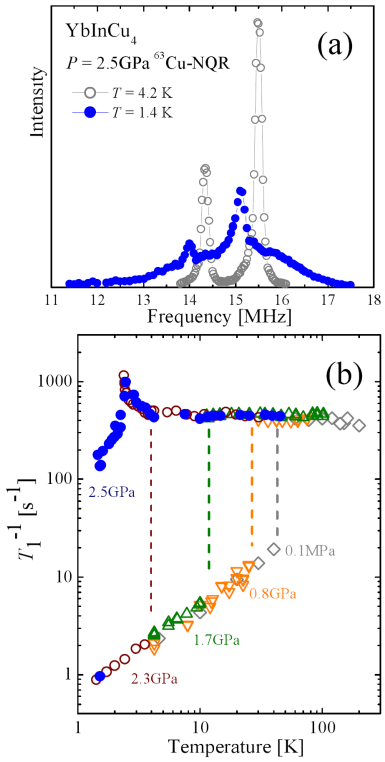

Fig. 6. (a) Cu-NQR lines at 2.5 GPa. (b) Temperature dependence of $1/T_1$ measure at 2.5 GPa (solid symbols), along with the data at ambient pressure, 0.8, 1.7 and 2.3 GPa.

MO phase*. Let us note that, because the ordered moments are not fully developed at the experimental lowest temperature of 1.4 K [2], the signal from the MO phase will become broader at lower temperatures. The IV phase signal is observed from 2.3 GPa to at least 2.6 GPa, the highest pressure of the present NQR experiment. In order to ensure the assignment of these resonance lines, we have measured T_1 at different frequencies: 15.49 MHz (PM phase) for $T > T_M$, whereas 16.0 MHz (MO phase) and 15.10 MHz (IV phase) for $T < T_M$. Just above T_M, $1/T_1$ shows a rapid increase upon cooling, consistent with the earlier report [1, 27]. The present result reveals a sharp peak at T_M, followed by a steep decrease below T_M. Such temperature dependence of $1/T_1$ is typical of the critical slowing down behavior that evidences a second-order like magnetic transition. On the other hand, $1/T_1$ measured at 15 MHz below T_M is in good agreement with the $1/T_1T \approx$ const law that is characteristic of the Fermi liquid behavior observed in the IV phase at lower pressures. Here, the T_1 decay curve consists of short and long components due to the overlap with the broad signal from the MO phase. While the MO phase is responsible for the short component, the long one probably arises from the IV phase.

One of the most remarkable pressure effects on this compound is that while T_V strongly depends on pressure, the magnetic properties of both PM and IV phases are insensitive to pressure, as indicated by the results of T_1. Beside, the significant difference in T_1 between the MO and IV phases around P_C strongly suggests that the transition between the IV and MO phases is of the first-order with pressure. The coexistence of the IV and MO phases in a rather wide pressure range also supports this. Since similar sudden appearance of the MO phase with pressure is also reported in other Yb-based materials such as $YbCu_2Si_2$ [28] and $YbRh_2Si_2$ [29], such behavior appears to be one of typical features of pressure-induced magnetism in strongly correlated Yb-based compounds, as well as the second-order like transition anticipated in $YbCu_5$.

4. Summary

The pressure effect on $YbCu_5$ and $YbInCu_4$ have been investigated by the NQR, NMR and resistivity measurements under pressure. The magnetic properties of $YbCu_5$ are well understood by considering chemical pressure of $P_0 = 5.6$ GPa with respect to a moderately heavy fermion compound $YbAgCu_4$. From the gradual suppression of the low-temperature Fermi liquid state with pressure, one can anticipate the second-order like nonmagnetic–magnetic transition around the pressure of 5–6 GPa in $YbCu_5$. For $YbInCu_4$, the direct observation of the NQR signal from the MO phase confirms magnetic ordering and the first-order nature of the transition between the IV and MO phases.

Acknowledgments

This work was partially supported by Grant-in-Aid for Scientific Research (No. 19540368) from the Ministry of Education, Culture, Sports, Science and Technology of Japan.

References

[1] T. Koyama, M. Nakamura, T. Mito, S. Wada, J.L. Sarrao, *Phys. Rev. B* **71**, 184437 (2005).

[2] T. Mito, M. Nakamura, M. Otani, T. Koyama, S. Wada, M. Ishizuka, M.K. Forthaus, R. Lengsdorf, M.M. Abd-Elmeguid, J.L. Sarrao, *Phys. Rev. B* **75**, 134401 (2007).

[3] N. Tsujii, J. He, F. Amita, K. Yoshimura, K. Kosuge, H. Michor, G. Hilscher, T. Goto, *Phys. Rev. B* **56**, 8103 (1997).

[4] Y. Ihara, private communication.

[5] I. Felner, I. Nowik, D. Vaknin, Ulrike Potzel, J. Moser, G.M. Kalvius, G. Wortmann, G. Schmiester, G. Hilscher, E. Gratz, C. Schmitzer, N. Pillmayr, K.G. Prasad, H. de Waard, H. Pinto, *Phys. Rev. B* **35**, 6956 (1987).

* From the broadened line, the internal field at the Cu-site is roughly estimated as ≈ 1 kOe at the lowest temperature measured. This value will be increased by further lowering temperature.

[6] I. Nowik, I. Felner, J. Voiron, J. Beille, A. Najib, E. du Tremolet de Lacheisserie, G. Gratz, *Phys. Rev. B* **37**, 5633 (1988).

[7] T. Mito, T. Koyama, M. Shimoide, S. Wada, T. Muramatsu, T.C. Kobayashi, J.L. Sarrao, *Phys. Rev. B* **67**, 224409 (2003).

[8] J.L. Sarrao, C.D. Immer, Z. Fisk, C.H. Booth, E. Figueroa, J.M. Lawrence, R. Modler, A.L. Cornelius, M.F. Hundley, G.H. Kwei, J.D. Thompson, F. Bridges, *Phys. Rev. B* **59**, 6855 (1999).

[9] C. Rossel, K.N. Yang, M.B. Maple, Z. Fisk, E. Zirngiebl, J.D. Thompson, *Phys. Rev. B* **35**, 1914 (1987).

[10] N. Tsujii, J. He, K. Yoshimura, K. Kosuge, H. Michor, K. Kreiner, G. Hilscher, *Phys. Rev. B* **55**, 1032 (1997).

[11] J.L. Sarrao, A.P. Ramirez, T.W. Darling, F. Freibert, A. Migliori, C.D. Immer, Z. Fisk, Y. Uwatoko, *Phys. Rev. B* **58**, 409 (1998).

[12] A. Iandelli, A. Palenzona, *J. Less-Common Met.* **25**, 333 (1971).

[13] J. Hornstra, K.H.J. Buschow, *J. Less-Common Met.* **27**, 123 (1972).

[14] B. Idzikowski, A. Jezierski, K. Nenkov, *J. Appl. Phys.* **85**, 4744 (1999).

[15] M. Reiffers, B. Idzikowski, J. Šebek, E. Šantavá, S. Ilkovič, G. Pristáš, *Physica B* **378-380**, 738 (2006).

[16] J.L. Sarrao, C.D. Immer, C.L. Benton, Z. Fisk, J.M. Lawrence, D. Mandrus, J.D. Thompson, *Phys. Rev. B* **54**, 12207 (1996).

[17] E. Bauer, R. Hauser, E. Gratz, K. Payer, G. Oomi, T. Kagayama, *Phys. Rev. B* **48**, 15873 (1993).

[18] T. Graf, R. Movshovich, J.D. Thompson, Z. Fisk, P.C. Canfield, *Phys. Rev. B* **52**, 3099 (1995).

[19] O. Trovarelli, C. Geibel, S. Mederle, C. Langhammer, F.M. Grosche, P. Gegenwart, M. Lang, G. Sparn, F. Steglich, *Phys. Rev. Lett.* **85**, 626 (2000).

[20] K. Ishida, K. Okamoto, Y. Kawasaki, Y. Kitaoka, O. Trovarelli, C. Geibel, F. Steglich, *Phys. Rev. Lett.* **89**, 107202 (2002).

[21] K. Kadowaki, S.B. Woods, *Solid State Commun.* **58**, 507 (1986).

[22] N. Tsujii, K. Yoshimura, K. Kosuge, *J. Phys., Condens. Matter* **15**, 1993 (2003), and references therein.

[23] J.L. Sarrao, A.P. Ramirez, T.W. Darling, F. Freibert, A. Migliori, C.D. Immer, Z. Fisk, Y. Uwatoko, *Phys. Rev. B* **58**, 409 (1998).

[24] I.V. Svechkarev, A.S. Panfilov, S.N. Dolja, H. Nakamura, M. Shiga, *J. Phys.: Condens. Matter* **11**, 4381 (1999).

[25] A. Uchida, M. Kosaka, N. Mori, T. Matsumoto, Y. Uwatoko, J.L. Sarrao, J.D. Thompson, *Physica B* **312-313**, 339 (2002).

[26] M. Hedo, Y. Uwatoko, T. Matsumoto, J.L. Sarrao, J.D. Thompson, *Acta Phys. Pol. B* **34**, 1193 (2003).

[27] Ben-Li Young, N.J. Curro, V.A. Sidorov, J.D. Thompson, J.L. Sarrao, *Phys. Rev. B* **71**, 224106 (2005).

[28] H. Winkelmann, M.M. Abd-Elmeguid, H. Micklitz, J.P. Sanchez, P. Vulliet, K. Alami-Yadri, D. Jaccard, *Phys. Rev. B* **60**, 3324 (1999).

[29] J. Plessel, M.M. Abd-Elmeguid, J.P. Sanchez, G. Knebel, C. Geibel, O. Trovarelli, F. Steglich, *Phys. Rev. B* **67**, 180403 (2003).